Figure 8 shows the neutral axis angular shift for both linear and incremental models as a function of rotational velocity.

DISCUSSION

The rather angular appearance of the flux lines shown in Figs. 5, 6, and 7 is due to both the small number of triangular meshes used, and the straight line interpolation procedure between nodes employed in the plotting routine. Both effects could be reduced at the expense of an increase in mesh number and computer time required for solution.

Comparison of Fig. 6a and 6b and Fig. 7a with 7b shows that the circular fields inside the rotating bar are strongest in the case of the incremental model approach whereas the neutral axis shift is greatest in the linear or direct superposition model. This may seem somewhat paradoxical, however, in the direct superposition model equation 6 results in a symmetrical current distribution with respect to the y axis, whereas in the incremental model the current distribution is not symmetrical because of the different magnitudes and directions of $B_1^1, B_2^1, \cdots, B_k^1$. Consequently, stronger internal circular fields do not necessarily correspond to a larger shift in the neutral axis.

In conclusion, it can be stated from this study that care should be taken in applying finite element techniques to the analysis of nonlinear magnetic structures such as electrical machines, where superposition of fields is contemplated. A comparison of neutral axis shifts in Fig. 8 shows clearly the degree of error involved in a direct superposition of main and cross fields in the case of a circular ferromagnetic bar rotating in a magnetic field.

REFERENCES

[1] A. M. Winslow, "Numerical Solution of the Quasi-linear Poisson Equation in a Nonuniform Triangular Mesh," *Journal of Computational Physics*, Vol. 1, Number 2, pp. 149-172, November 1966.

[2] M. V. K. Chari and P. Silvester, "Finite-Element Analysis of Magnetically Saturated D-C Machines," *IEEE Transactions on Power Apparatus and Systems*, Vol. PAS-90, Number 5, pp. 2362-2371, September/October 1971.

[3] Y. K. Hong and E. K. Stefanakos, "Magnetic Field Distribution in a Ferromagnetic Conductor," *IEEE Transactions on Magnetics*, Vol. MAG-9, Number 2, pp. 111-113, June 1973.

[4] H. H. Woodson and J. R. Melcher, *Electromechanical Dynamics*, New York: John Wiley & Sons, 1968, pp. 330-403, Vol. II.

[5] O. W. Anderson, "Iterative Solution of Finite Element Equations in Magnetic Field Problems," Conference Paper, IEEE PES Summer Meeting, San Francisco, Cal., July 9-14, 1972.

[6] S. V. Ahamed and E. A. Erdelyi, "Flux Distribution in D.C. Machines On-Load and Overloads," *IEEE Transactions on Power Apparatus and Systems*, Vol. PAS-85, Number 9, pp. 960-967, September 1966.

[7] E. A. Erdelyi, S. V. Ahamed and R. D. Burtness, "Flux Distribution in Saturated D.C. Machines at No-Load," *IEEE Transactions on Power Apparatus and Systems*, Vol. PAS-84, pp. 375-381, May 1965.

A Field-Theoretical Approach to Magnetic Induction Heating of Thin Circular Plates

M. S. ADLER

Abstract — A field-theoretical approach is used to analyze the subject of magnetic induction heating of thin circular plates by planar coils. Closed-form solutions for the electric and magnetic fields are found to the basic field problem of a single circular loop carrying current at a frequency ω in the presence of a plate characterized by a permeability μ and conductivity σ. By using these fields, expressions are derived for the complex Poynting vector at the surface of the plate, and for the induced EMF in the coil. The theory is extended to include multiturn coils and a field-dependent permeability, and a specific multiturn coil and plate combination is chosen as an example. The complex amplitude of the magnetic field and the Poynting vector are calculated along the surface of the plate using iterative methods to assure self-consistency with the field dependent permeability of the plate. By using Fourier transform techniques, the transient coil current and coil voltage waveforms are calculated under the experimental conditions used to take data on the sample coil and plate. The absorbed power is calculated from these waveforms and is found to be within 10 percent of the measured power absorption for all levels of operation from 50 to 2000 W. The calculated coil current waveform is compared with the measured waveform and is found to be in very good agreement in both shape and period.

Manuscript received February 4, 1974; revised April 4, 1974.

The author is with General Electric Company Research and Development Center, Schenectady, N.Y. 12301.

I. INTRODUCTION

In this paper a field-theoretical approach will be used to analyze the subject of the magnetic induction heating of thin

circular plates by planar coils. A great deal has been written on the subject of induction heating and its industrial applications but the geometries usually considered are those of either a solid cylinder or a rectangular slab [1], [2]. A recent paper by Moreland [3] considers the circular plate geometry but is mainly qualitative in its approach. The purpose of this paper will be to develop an analytical model that will both engender understanding of the physical processes involved in induction heating and that can be used in full quantitative detail to design induction heating systems optimally using this geometry.

The paper is divided into two sections. In the first section the field-theoretical model is developed in which a closed-form solution is sought to the basic field problem of a single circular loop carrying current at an angular frequency ω in the presence of a semi-infinite plate characterized by a permeability μ and a conductivity σ. In the second section it is shown that the solution to this problem is a good approximate solution to the field problem of circular plate slightly larger than the coil. Expressions are formulated for the complex amplitudes in the sinusoidal steady state of the electric and magnetic fields. By using these fields an expression is derived for the complex Poynting vector at the surface of the plate which gives the distribution of the power flow into the plate and can be integrated to find the total power absorbed in the plate. In addition, an expression is derived for the complex amplitude of the induced voltage in the coil which, to within a constant, is the impedance of the loaded coil. Finally, techniques are discussed for treating a nonlinear permeability in the scope of an otherwise linear theory.

In the second section the theory is extended to include multiturn coils. A specific coil-plate combination for which data were taken is used as a vehicle for presenting the results of the theory. The complex amplitudes of the magnetic field and the Poynting vector are calculated along the surface of the plate using iterative methods to assure self-consistency with the field dependent permeability of the plate. The complex impedance of the multiturn coil is formed and Fourier techniques are used to calculate the coil current and coil voltage waveforms and the absorbed power under the experimental conditions of a step voltage excitation of the tuned circuit formed by the coil-plate combination and a capacitor. The calculated absorbed power and current waveforms are then compared with experiment and are found to be in good agreement.

II. SOLUTION TO THE FIELD PROBLEM

A. Problem Definition

The basic field problem consists of a single circular coil of radius R carrying a current I at frequency ω separated by a distance h from a plate of radius $R_p > R$ with conductivity σ and permeability μ. Neglecting for the moment nonlinearity and hysteresis effects in ferrous metals, superposition can then be used to obtain the fields for a coil consisting of many turns placed at various radii R and distances h from the plate. This will be done in the next section. The methods to be used will lead to a solution that, although approximate, should represent the actual fields very well. Theoretical arguments and experimental evidence to support this contention will be given in this section and the next.

To solve the basic field problem, the following equation for the vector potential must be solved [4]

$$\nabla^2 \vec{a}(r,t) - \mu\epsilon \frac{\partial^2 \vec{a}(r,t)}{\partial t^2} - \mu\sigma \frac{\partial \vec{a}(r,t)}{\partial t} = 0. \tag{1}$$

For a metal at the frequency of interest ($f = 30$ kHz), the first time-dependent term is much smaller than the second term and can be neglected. In addition, the geometry is cylindrically symmetric so that only the $\vec{a}_\varphi$ component of the vector potential need be considered. Finally, assuming harmonic variation of the fields (Fourier analysis will be done later) the field equation to be solved in the plate becomes

$$\frac{\partial^2 A_\varphi(r,z)}{\partial z^2} + \frac{\partial}{\partial r}\left(\frac{1}{r}\frac{\partial}{r}(rA_\varphi(r,z))\right) - i\omega\mu\sigma A_\varphi(r,z) = 0 \tag{2}$$

where $\vec{a}(r,z,t) = \hat{i}_\varphi A_\varphi(r,z)\, e^{i\omega t}$ and $A_\varphi(r,z)$ is the complex amplitude of the vector potential. Outside the metal both time-dependent terms can be neglected since the wavelength of electromagnetic waves in air at 30 kHz is much larger than the size of the coil ($\lambda = 10^4$ m compared to the radius $R = 0.1$ m) leaving the first two terms in (2) as the field equation to be solved.

Rather than attempt to solve the field problem for a finite plate, a closed-form solution will be sought to the more tractable field problem where the plate is infinite in extent (see Fig. 1). This solution should be a good approximate solution to the problem with a finite plate slightly larger than the coil since, for the geometries of interest, the plate is very close to the coil ($h \ll R$) and the fields at the plate surface fall off very rapidly for radii greater than the outer radius of the coil. This issue will be discussed in the next section in the context of a specific example.

B. Method of Solution

The approach to be taken will be to use a variation on the method of images [5]. If the plate were perfectly conducting, the problem would be quite simple as there would be no fields within the plate and the fields on the outside would be given by the superposition of the fields of the actual coil and of an image coil placed equidistantly from the surface of the plate at $z = h$ (see Fig. 1) but with an oppositely directed current flow. However, for the case of interest where the plate has finite conductivity, fields will exist inside of the plate as well, and the problem becomes much more complicated.

A set of trial solutions for the vector potential inside and outside of the plate are given in (3) and (4). The basis for these choices of functions will be discussed below.

$$A_{\varphi o}(r,z) = \frac{I}{2\pi} k\, \mu_o \left(\frac{R}{r}\right)^{1/2} \times \left[\left(\frac{2}{k^2} - 1\right) \times K(k) - \frac{2}{k^2} E(k)\right] \quad \text{(outside)}$$
$$+ \frac{I'}{2\pi} k'\, \mu_o \left(\frac{R}{r}\right)^{1/2} \times \left[\left(\frac{2}{k'^2} - 1\right) \times K(k') - \frac{2}{k'^2} E(k')\right] \tag{3}$$

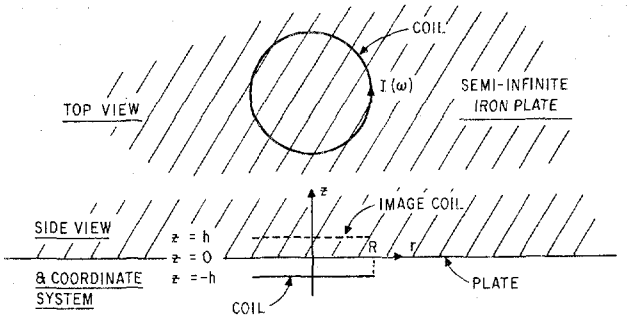

Fig. 1. Geometry of the basic field problems to be solved.

$$+\frac{I''}{4\pi}\times\frac{\mu_o}{R^{1/2}r^{3/2}}\times k'\times(z-h)\times\left[\left(\frac{1-\frac{k'^2}{2}}{1-k'^2}\right)\times E(k')-K(k')\right]$$

$$A_{\varphi i}(r,z)\ (\text{inside}) = \frac{I'''\mu_o}{4\pi R^{1/2}r^{3/2}}\times k\,(z+h)\times\left[\left(\frac{1-\frac{k^2}{2}}{1-k^2}\right)\times E(k)-K(k)\right]\times e^{-\sqrt{\frac{\omega\mu\sigma}{2}}(1+i)z} \quad (4)$$

$$+\frac{I^{\text{iv}}}{4\pi R^{1/2}r^{3/2}}\times k'\times(z-h)\times\left[\left(\frac{1-\frac{k'^2}{2}}{1-k'^2}\right)\times E(k')-K(k')\right]\times e^{-\sqrt{\frac{\omega\mu\sigma}{2}}(1+i)z}$$

where

$$k^2 = \frac{4rR}{(r+R)^2+(z+h)^2}$$

$$k'^2 = \frac{4rR}{(r+R)^2+(z-h)^2}.$$

In these equations r, R, h, and z are defined in Fig. 1, $K(k)$ and $E(k)$ are the complete elliptic integrals of modulus k of the first and second kinds respectively, μ_o is the permeability of free space, μ is the permeability of the plate, σ is the conductivity of the plate, ω is the angular frequency, I is the actual coil current, and I', I'', I''', and I^{iv} are undetermined constants. The first term in (3) is the vector potential of a circular current carrying ring [6] of radius R located at $z=-h$. The second term is the vector potential of an image coil placed at $z=h$ but with the current I' unspecified at this time. The third term is the derivative with respect to z of the second term but also with an undetermined current I''. It should be noted that since the operator $\partial/\partial z$ commutes with the wave equation (2), that is, it can be operated through the existing operators without changing them, the derivative with respect to z of any solution to the equation is also a solution. (The same cannot be said about derivatives with respect to r.)

The solutions for the vector potential inside the metal shown in (4) are product functions between a term similar to the last term in (3) (to be referred to as the coil factor) and a complex exponential in the variable z. In the first term in (4) the modulus k is referenced to the actual coil and in the second term the modulus k' is referenced to the image coil at $z=h$. These product functions are not exact solutions to the wave-equation (2), but are, in fact, very good approximate solutions. The coil factor will vanish when acted upon by the first two terms and the exponential factor will vanish when acted upon by the first and last terms of (2). The problem arises because both factors depend on the variable z so there is an additional cross term left over involving the product of the first derivatives with respect to z of each of the factors. However, explicit evaluation has shown that this term is only 0.03% of the second derivative of the exponential term and can thus safely be neglected. Some insight can be obtained into this by noting that the factor $\sqrt{\omega\mu\sigma/2}$ appearing in the exponential is actually the reciprocal of the classical skin depth and for an iron plate at 30 kHz the skin depth is only 30 μm. Therefore, neglecting the above cross term in determining a solution to (2) is equivalent to noting that in the distance of several skin depths over which the surface fields will completely vanish due to the skin effect, the factor derived from the magnetostatic current ring solution will remain virtually constant.

C. Boundary Conditions

It now is necessary to show that the fields derived from the vector potentials of (3) and (4) can satisfy the boundary conditions at the air-metal interface and to determine in the process the values of the constants appearing in these equations. The boundary conditions to be imposed are that the tangential magnetic field H and electric field E and the normal magnetic flux density B are continuous at the interface.

The boundary condition for the radial magnetic field intensity is given as

$$\frac{1}{\mu_o}\left(\frac{\partial A_{\varphi o}(r,z)}{\partial z}\right)_{z=0} = \frac{1}{\mu}\left(\frac{\partial A_{\varphi i}(r,z)}{\partial z}\right)_{z=0} \quad (5)$$

and the boundary conditions for the z directed magnetic flux density is given

$$\frac{1}{r}\left(\frac{\partial}{\partial r}(rA_{\varphi o}(r,z))\right)_{z=0} = \frac{1}{r}\left(\frac{\partial}{\partial r}(rA_{\varphi i}(r,z))\right)_{z=0} \quad (6)$$

Since the boundary conditions must be satisfied over the entire interface, fields on both sides of the interface must have the same functional dependence on the radius r. Thus, the reasons for the choice of the particular trial functions in (3) and (4) are now seen to be due to the requirements of satisfying the boundary conditions for the two magnetic fields which relate to different derivatives of the vector potential. Satisfaction of the boundary conditions leads to the following values for the four unknown constants

$$I' = -I \quad (7)$$

$$I'' = -2\sqrt{\frac{\mu}{2\omega\sigma}}\frac{1}{\mu_0}(1-i)I \quad (8)$$

$$I''' = -\sqrt{\frac{\mu}{2\omega\sigma}}\left(\frac{\mu-\mu_0}{\mu_0^2}\right)(1-i)\,I \tag{9}$$

$$I^{iv} = -\sqrt{\frac{\mu}{2\omega\sigma}}\left(\frac{\mu+\mu_0}{\mu_0^2}\right)(1-i)\,I. \tag{10}$$

The boundary condition on the tangential electric field is also met by this choice of constants since the constraint imposed is identical to that given in (6) for the magnetic flux density. It should also be noted that making either σ or ω very large causes the constants I'', I''', and I^{iv} to vanish and the two remaining terms are just those that make up the solution for a coil and a perfectly conducting plate previously discussed.

The formal expressions for the fields can now be obtained. The radial magnetic field and the φ component of the electric field outside the plate are given by

$$\begin{aligned} H_r(r,z) = {} & \frac{I}{4\pi R^{1/2} r^{3/2}} \times \left[(z+h)\,k \times \left(\left(\frac{1-\frac{k^2}{2}}{1-k^2}\right) \times E(k) - K(k)\right) - (z-h)k' \times \left(\left(\frac{1-\frac{k'^2}{2}}{1-k'^2}\right) \times E(k') - K(k')\right)\right] \\ & - \frac{I(i-1)}{4\pi R^{1/2} r^{3/2}} \times \sqrt{\frac{2}{\omega\mu\sigma}} \times \frac{\mu}{\mu_0} \times \left(\frac{k'^3}{1-k'^2}\right) \\ & \times \left[-k'^2 \times \left(\frac{1-\frac{k'^2}{2}}{1-k'^2}\right) \times E(k') - \frac{k'^2}{4} \times K(k') + \left(\frac{r}{4R} + \frac{R}{4r}\right) \times \left(\left(\frac{1-k'^2+k'^4}{1-k'^2}\right) \times E(k') - \left(1-\frac{k'^2}{2}\right) \times K(k')\right)\right] \end{aligned} \tag{11}$$

$$\begin{aligned} E_\varphi(r,z) = {} & -i\omega I \frac{\mu_o}{2\pi} \left(\frac{R}{r}\right)^{1/2} \\ & \times \left[k \times \left(\left(\frac{2}{k^2}-1\right) \times K(k) - \frac{2}{k^2} \times E(k)\right) - k' \times \left(\left(\frac{2}{k'^2}-1\right) \times K(k') - \frac{2}{k'^2} \times E(k')\right)\right] \\ & + \frac{I(1+i)\,\omega\mu}{4\pi R^{1/2} r^{3/2}} \times \sqrt{\frac{2}{\omega\mu\sigma}} \times (z-h) \times k' \\ & \times \left[\left(\frac{1-\frac{k'^2}{2}}{1-k'^2}\right) \times E(k') - K(k')\right] \end{aligned} \tag{12}$$

where

$$k'^2 = \frac{4Rr}{(r+R)^2 + (z-h)^2} \quad \text{and} \quad k^2 = \frac{4Rr}{(r+R)^2 + (z+h)^2}.$$

The z component of the magnetic field and the fields inside the plate are not needed in the subsequent development and are consequently not given.

D. Induced Coil Voltage

Having expressions for the fields it now becomes possible to calculate several items of experimental interest such as the induced EMF in the coil. The procedure amounts to integrating the z directed magnetic flux density over the area enclosed by the coil with the result being

$$v = \frac{d\varphi}{dt} = i\omega(2\pi r A_{\varphi o}(r,z)). \tag{13}$$

Upon evaluation, the induced coil voltage is given as

$$\begin{aligned} v = {} & i\omega\mu_o I \times \left[R \times \left\{k \times \left(\left(\frac{2}{k^2}-1\right) \times K(k) - \frac{2}{k^2} \times E(k)\right) - k' \times \left(\frac{2}{k'^2}-1\right) \times K(k') - \frac{2}{k'^2} \times E(k')\right)\right\}\right] + (i+1) \\ & \times \omega\mu I \times \sqrt{\frac{2}{\omega\mu\sigma}} \times \frac{hk'}{R} \times \left[\left(\frac{1-\frac{k'^2}{2}}{1-k'^2}\right) \times E(k') - K(k')\right] \end{aligned} \tag{14}$$

where

$$k' = \frac{2R}{\sqrt{4R^2 + 4h^2}} \qquad k = \sqrt{\frac{4(R-\Delta r)R}{(2R-\Delta r)^2}}$$

where Δr is taken to be the radius of the coil wire. Evaluation cannot actually be made right at $r = R$ since the first term in (14), which represents the self-inductance of the coil, would be infinite. For $\Delta r \ll R$ the effect of including the wire size on the other terms is negligible and thus has not been included in the above.

The second term in (14) is similar in form to the self-inductance term but opposite in sign and does not depend on the electrical and magnetic properties of the plate. This term together with the self-inductance term represents the total coil impedance when the plate is of very high conductivity and low permeability. The final term which has equal lossy and reactive components is present when the fields penetrate into the plate and power is absorbed.

E. Poynting Vector

The real part of the complex Poynting vector gives the distribution of power flow into the plate and can be integrated to give an alternate way, that is other than (14), of calculating the absorbed power in the plate. For our geometry, the z component is the only component of the real part of the complex Poynting vector that exists and is given by

$$\mathrm{Re}\,(S_z(r,z)) = -\frac{1}{2}\,\mathrm{Re}\,(E_\varphi(r,z) \times H_r^*(r,z)). \tag{15}$$

By including (11) and (12) for the fields, this expression was evaluated at the surface of the plate and is given by

$$\mathrm{Re}\,(S_z(r,o)) = I^2\,\omega\mu \times \sqrt{\frac{2}{\omega\mu\sigma}} \times \frac{h^2k^2}{16\pi^2 Rr^3} \times \left[\left(\frac{1-\frac{k^2}{2}}{1-k^2}\right) \times E(k) - K(k)\right]^2 \tag{16}$$

where

$$k = \sqrt{\frac{4Rr}{(R+r)^2 + h^2}}.$$

F. Nonlinearities and Techniques

If one is completely rigorous and also insists on using a nonlinear parameter such as a magnetic-field-dependent permeability in an otherwise linear system, then a linear theory, such as that in this section, is not valid. Furthermore, even if it were valid it would not be possible to superimpose solutions to arrive at an answer to a composite structure. However, believing an approximate nonlinear solution is better than neglecting the nonlinearities altogether, two techniques were used to account for some aspects of the nonlinear nature of the problem and otherwise preserve the basis of previously developed linear theory.

In this section the solution to the field problem was developed for a generalized complex sinusoid at a specific angular frequency ω, and, as such, the fields were characterized by their complex amplitudes of this sinusoid. Consequently, it is more appropriate to use an average permeability associated with the amplitude of a sinusoid rather than one associated with the instantaneous value of the field at any point in time. Therefore, an average permeability $\mu_{av}(H)$ is defined as

$$\mu_{av}(H) = \frac{2\omega}{\pi} \int_0^{\frac{\pi}{2\omega}} \frac{B(H \sin \omega t)}{H \sin \omega t} dt \qquad (17)$$

where $B(H)$ is the value of the magnetic flux density at a particular field strength H. A further discussion of this average permeability will be given later. It should be noted that the nonlinear permeability will result in fields at higher harmonics being present and these fields will in turn induce voltages in the coil. However, study of (15) and (11) and (12) for the fields reveals that, to first order at least, no power will be absorbed at these higher harmonics. Furthermore, if the coil is part of a tuned circuit at frequency ω, as is the case for the example in the next section, these higher harmonic voltages will be severely attenuated and should not affect the overall solution.

The second issue is that of superposition of fields when the plate has a nonlinear permeability. Superposition in the normal sense is not possible in a nonlinear system and can only be done if it is treated self-consistently. The approach to be taken here will be to insure always, through iteration of the solution, that at all points along the surface of the plate the permeability used to calculate the fields is the permeability that is associated with those fields.

III. FIELD AND POWER CALCULATIONS AND A FOURIER TRANSFORM APPROACH TO COIL MODELING

A. Calculations on the Sample Coil

In this section, field and power calculations and measurements are presented for the coil and plate shown in Fig. 2. The loaded coil and a capacitor form the tuned circuit shown in Fig. 3. In the experiment the circuit was driven by what amounted to a step voltage source and the power delivered to the circuit was measured as a function of the peak current in the current response.

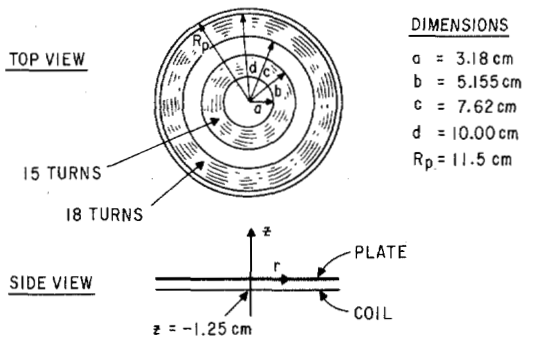

Fig. 2. Geometry of the coil and plate used in experimental testing.

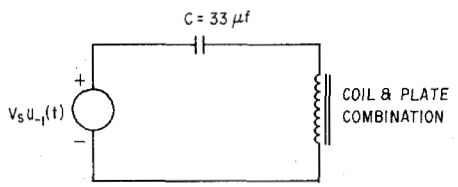

Fig. 3. Equivalent circuit used in experimental testing.

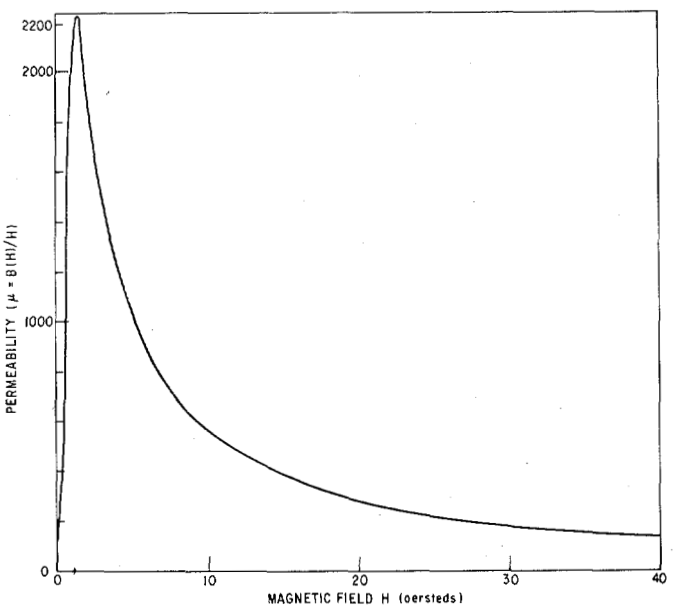

Fig. 4. Permeability of the iron plate as a function of magnetic field.

The conductivity of the plate which was made from cold-rolled steel was taken as

$$\sigma = 1.0 \times 10^5 \text{ (ohm-cm)}^{-1}.$$

The actual permeability ($\mu(H) = B(H)/H$) of the plate material is not known and the curve shown in Fig. 4 will be used instead. The shape of this curve is that for ordinary transformer steel [7] but the curve has been scaled by a factor of 2.5 so that the maximum permeability is approximately that of cold rolled steel [7] ($\mu_{max} = 2000$).

In Fig. 5 the results of the steady-state field calculations for the coil in Fig. 2 are shown with a current $I = 51$ A and

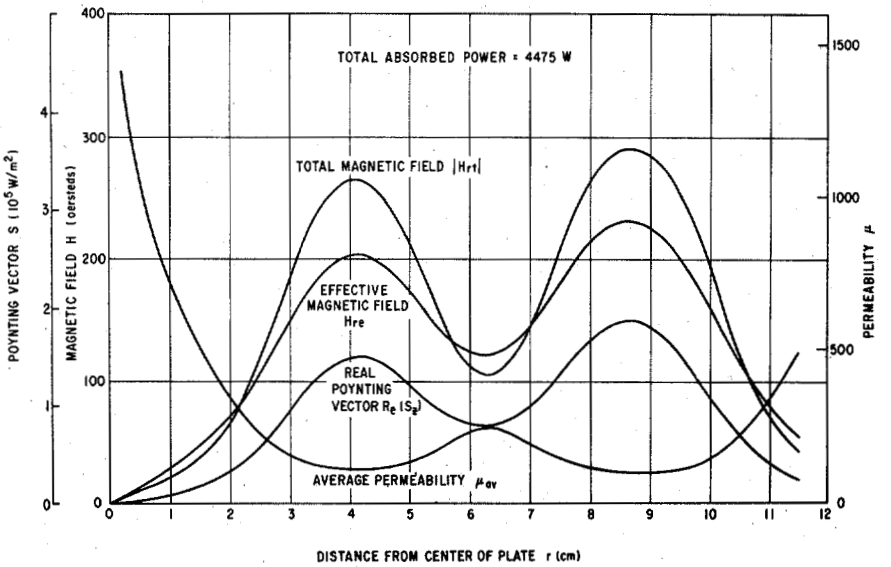

Fig. 5. Magnetic fields, Poynting vector, and average permeability at the surface of the plate for the sample coil with a current of 51 A.

$f = 30.0$ kHz. All calculations are for $z = 0$, the surface of the plate, and are shown as a function of the distance r from the center of the plate. Included in Fig. 5 are the magnitude of the total radial magnetic field $|H_{rt}(r)|$, the part of the field in phase with the current and contributing to power absorption $H_{re}(r)$, the real part of the complex Poynting vector Re $(S_z(r))$, and the average permeability of the plate (as defined in (17)) that achieved self-consistency with the calculated total field $\mu_{av}(H_{rt})$, that is $H_{rt} = H_{rt}(\mu_{av}(H_{rt}))$. It is worth observing that the field H_{re} is simply twice the field that would be present at $z = 0$ if the plate were removed and would be the total radial field if the plate were a perfect conductor. The total absorbed power in the plate was $P = 4475$W. As can be seen, the variation in the total magnetic field as a function of radius is accompanied by an inverse type of variation in the permeability $\mu_{av}(H_{rt})$. Since the real part of the Poynting vector is proportional to the square root of the permeability (see (16)), the variation of $\mu_{av}(H_{rt})$ somewhat compensates for the variation in the magnetic field and results in a more uniform distribution of input power to the plate. In addition, the inverse variation of the permeability also smooths the variations in the total magnetic field since H_{rt} is also proportional to the square root of the permeability (see (11)).

B. Complex Impedance of the Coil

Equation (14) of the last section and the associated discussion will be used as a guide in forming the complex impedance of the loaded coil. This equation shows that there are three reactive terms and one lossy term. The first two terms represent inductances and the value of these terms can be calculated for a multiturn coil by summing the flux linked by each coil, produced by fields of all of the coils under the condition that the plate is of infinite conductivity. The flux produced by a single coil carrying one ampere of current located at R_i, and linking an area $(R_j - \Delta r)^2$ is given by

$$\varphi_{ij}(R_i, R_j) = \mu_o R_i^{1/2} \times (R_j - \Delta r)^{1/2} \times \left[k \times \left(\left(\frac{2}{k^2} - k\right) \times K(k) - \frac{2}{k^2} \times E(k)\right) - k' \times \left(\left(\frac{2}{k'^2} - 1\right) \times K(k') - \frac{2}{k'^2} E(k')\right)\right] \tag{18}$$

where

$$k = \sqrt{\frac{2(R_j - \Delta r) R_i}{(R_j - \Delta r + R_i)^2}} \qquad k' = \sqrt{\frac{2(R_j - \Delta r) R_i}{(R_j - \Delta r + R_i)^2 + 4h^2}}$$

and where Δr is the radius of the wire used to make the coil. If one now sums $\varphi_{ij}(R_i, R_j)$ over all of the coils R_i, the total flux linking a coil located at R_j results. Then, if this is done for each of the coils and the results summed, the total flux linked is calculated. This procedure was done for the coil in Fig. 2 with the result that the self-inductance term was

$$L_{11} = 154.2\ \mu\text{H}$$

and the total for both terms in (18) was

$$L_{11} - L_{12} = 66.7\ \mu\text{H}.$$

The measured value for the self-inductance was

$$L_{11} = 142\ \mu\text{H}$$

and the measured inductance when an aluminum plate was located 1.25 cm above the coil, thus approximating the highly conducting-low permeability plate, is given as

$$L_{11} - L_{12} = 67\ \mu\text{H}.$$

As can be seen, the agreement is quite good.

The values for the lossy term and the third term in (14) are evaluated using the results of the field and power calculations

shown in Fig. 5. This is done by noting that the fourth term in (14) is a resistance in the sinusoidal steady state, and the power dissipated by this resistance is $P = 1/2\, I^2 R$. Since the only loss in the system is the power dissipated in the plate, the integral of the real part of the Poynting vector over the area of the plate must be identical to the power dissipated in the lossy term in (14) and can be used to infer the equivalent coil resistance for examples with nonlinearities and complicated geometry. This method was explicitly tested for the case of a single coil and plate (R = 10 cm, h = 1.25 cm) where the permeability was constant (μ = 1000). The results were that the two values of resistance were identical when the integration was extended to twice the coil radius and differed by only 3% when the "plate radius" was just 20% larger than that of the coil. With this justification, the equivalent resistance in the sinusoidal steady state at frequency f = 30 kHz is shown in Fig. 6 as a function of the complex amplitude of the current. As can be seen, the resistance is quite nonlinear changing by a factor of two in the range between 10 and 60 A.

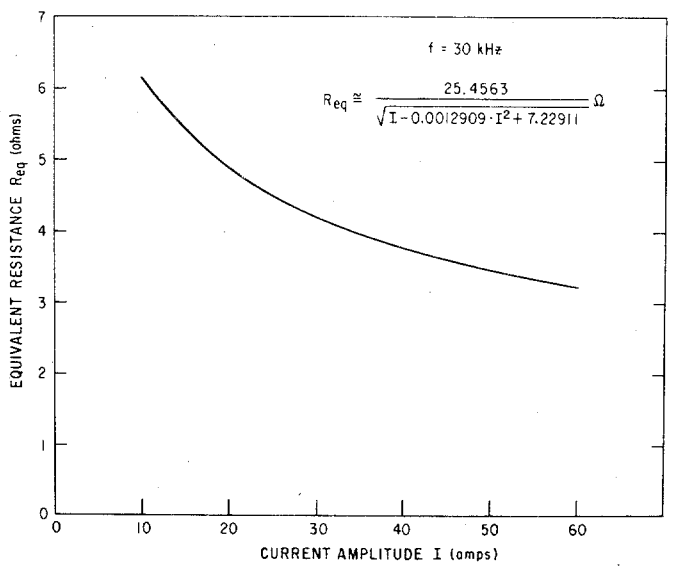

Fig. 6. Equivalent resistance of the loaded coil as a function of the amplitude of a 30 kHz sinusoidal current.

The Fourier transform of the impedance of the coil can now be formed and is given as

$$Z(\omega) = i\omega L + \frac{i\omega}{\sqrt{|\omega|}} X(I) + \sqrt{|\omega|}\, X(I) \qquad (19)$$

where $X(I) = R(I) / \sqrt{2\pi \times 30\ \text{kHz}} = R(I) / 434.2$ and $L = L_{11} - L_{12} = 66.7 \times 10^{-6}$ H. As can be seen from (14),it was necessary to divide $R(I)$ by the square root of the angular frequency that was used to formulate $R(I)$ in order to include all of the correct frequency dependent behavior in the transform. Also in (19), the use of the absolute value of ω is necessary to preserve the correct behavior of the transform under reversal of the sign of ω.

C. Comparison Between Theory and Experiment

The theoretical and experimental data on the power absorbed by the coil-plate combination as a function of the peak current is shown in Fig. 7. The experimental data is the input power into the tuned circuit in Fig. 3, as a function of the peak current sensed by a 0.021-Ω resistor and measured on an oscilloscope. External circuitry reset the circuit 34 μs after the start of the voltage step and the entire sequence was repeated every 50 μs. The theoretical curve was obtained by calculating both the coil current and in-phase voltage with inverse Fourier transforms using (19) and integrating the product up to t = 34 μs and normalizing by the repetition rate T = 50 μs. Because of the nonlinearity in the expression for the coil impedance in (19), it was necessary to iterate the resulting current at each instant in time to assure self-consistency. The peak current was monitored during the calculation. As can be seen, the agreement between theory and experiment is within 10 percent. It should be emphasized that the theory does not represent a fit of the data in any way. Because of the nonlinearity of the equivalent resistance shown in Fig. 6, a linear circuit model will never be able to predict accurately the behavior of the loaded coil.

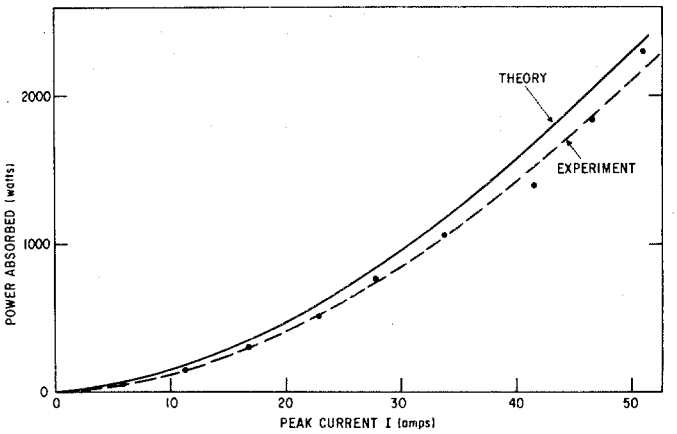

Fig. 7. Theoretical and experimental curves of the absorbed power in the plate as a function of the peak in the current response.

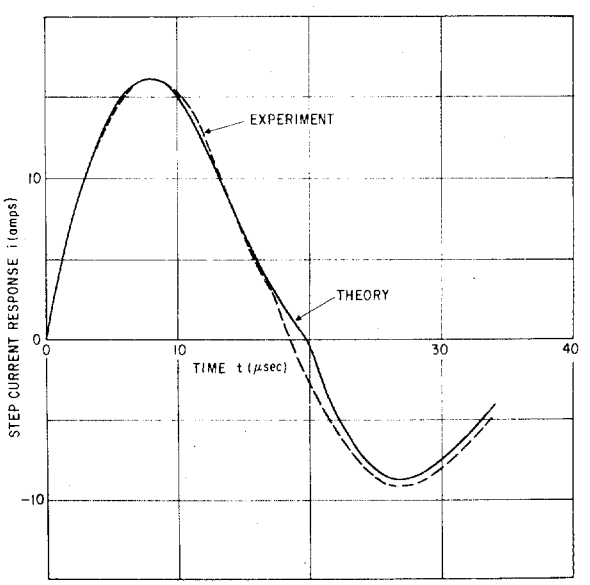

Fig. 8. Comparison between the experimental and theoretical current-response waveforms.

In Fig. 8 is shown a drawing of an oscilloscope picture of a typical current response to a step function of voltage (labeled experiment). As can be seen, there is a small "wrinkle" in the waveform at $t = 17$ μs. Also shown in Fig. 8 is the theoretical current response that was calculated using the inverse Fourier transform as above. The two waveforms are quite similar in shape and have identical periods. However, the theoretical curve exhibits slightly more damping and a more pronounced "wrinkle". This "wrinkle" has been shown to occur as a result of the nonlinearity in the function $X(I)$ appearing in the Fourier transform in (19). Improved agreement could be achieved by decreasing the overall size of the permeability in Fig. 4 as this will have the effect of reducing the amount of nonlinearity and decreasing the damping. A decrease in the damping will also have the effect of bringing the calculated power curve even more in line with the measured curve in Fig. 7. A change in the shape of the permeability curve will also be necessary if one insists on 100 percent accuracy in modeling the "wrinkle" in the experimental waveshape in Fig. 8. The closest approximation to the actual shape has been achieved by including hysteresis effects. However, doing this has the effect of substantially increasing the complexity of the calculation without materially improving other aspects of the results.

D. Discussion of the Approximations in the Theory

The theory given in this paper is an approximate one with the approximations falling into two classes: those associated with the solution of the linear field problem and those used to include a field dependent permeability into an otherwise linear theory. In the first class, two approximations were made as discussed in Section II of the paper. The first of these was that the z coordinate dependence of the fields inside the plate is dominated by the exponential "skin effect" type of variation and it was shown that this is indeed a good approximation. A second approximation was that the solution to the field problem with a semi-infinite plate would be a good approximation to the solution of the field problem for a finite plate that was larger in radius than the coil and located a small distance above the coil. Some comment will now be made on this.

For the example discussed in this section where the coil radius is 10 cm and the coil-plate separation is 1.25 cm, the power absorbed by the semi-infinite plate within the plate radius of 11.5 cm is 97 percent of the power absorbed by the entire plate. It is thus likely that the theory presented here when applied to this finite plate will not be in error by more than 3 percent in the power absorbed. The error could possibly be less since the integrated power within the plate radius should be closer to the true power absorbed by the finite plate than that absorbed by the entire semi-infinite plate. The calculated fields themselves should be accurate within the coil radius and undoubtedly largely in error outside the plate radius. However, these fields are quite small and of little interest in themselves.

Some comment should also be made about the approximate technique used in treating the nonlinear permeability and, in particular, the method of formulating the average permeability shown in (17). The entire concept of this average permeability is an approximation but the method used here is probably not the best that could be done, in general. The problem arises because in forming the Poynting vector at the plate surface when calculating the absorbed power, the surface permeability as determined by the surface fields is used. The theory inherently assumes that the permeability is the same inside the plate and, since the fields are decreasing in strength, this will not actually be the case. Consequently, an additional average of the permeability should be made with the average weighted by the absorbed power density within the plate. This was not done for the example given here because, with the uncertainties in the permeability curve that was used, this additional refinement did not seem worthwhile.

IV. SUMMARY

In this paper a comprehensive model for the induction heating of a circular plate by a planar coil has been developed using a field-theoretic approach. Closed-form expressions were derived for the complex amplitudes in the sinusoidal steady state for the electric and magnetic fields, the real part of the Poynting vector, and the induced EMF in the coil. A nonlinear dependence of the plate permeability on magnetic field was incorporated into the model and a specific multiturn coil was used in an experimental test of the theory. The nonlinear complex coil impedance was formed, and using a self-consistent application of Fourier integral techniques the absorbed power was calculated. The results agreed with measurements on the actual circuit within 10% over the entire range of power levels tested (50-2000 W). Over the same range of power levels the equivalent coil resistance at 30 kHz was found to change by a factor of more than two. This large nonlinearity and the fact that the coil impedance depends on the square root of the frequency indicates the futility of attempting to use a linear circuit to model the coil. A comparison was also made between the theoretical current waveform and the measured current waveform and they were found to be in excellent agreement in both shape and period including the presence of a small inflection.

ACKNOWLEDGMENT

I wish to credit and thank M. Bloomer and M. Ketchum for making the measurements for this paper and for their helpful comments and discussion.

REFERENCES

[1] P. G. Simpson, *Induction Heating Coil and System Design*, (McGraw-Hill, Inc., New York) 1960.
[2] J. D. Lavers and P. P. Biringer, "Induction Heating Calculations – the effect of Coil Geometry," *IEEE Conference Record 5th Annual Meeting – Industry and General Applications Group*, Oct. 5-8, 1970.
[3] W. C. Moreland II, *IEEE Trans. on Industry Appl.* IA-9, 81-85 (1973).
[4] J. A. Stratton, *Electromagnetic Theory* (McGraw-Hill, Inc., New York) 1941, p. 27, Eq. 28.
[5] *ibid*, p. 263, problem #3, #4.
[6] *ibid*, p. 193-194.
[7] *Handbook of Chemistry and Physics*, R. C. Weast, Ed. (Chemical Rubber Co., Cleveland), 1972, 53rd Edition, p. E108.